Experimental Control and Statistical Analysis of Thermal Conductivity in ZnO-Benzene Multilayer Thin Films

Fabian Krahl,[1] Ashutosh Giri[2,3], Md Shafkat Bin Hoque[2], Linda Sederholm[1], Patrick E. Hopkins[2,4,5], and Maarit Karppinen[1]*

[1]Aalto University, Department of Chemistry and Materials Science, Fi-00076 Aalto, Finland

[2]University of Virginia, Department of Mechanical and Aerospace Engineering, Charlottesville, VA 22904, USA

[3]University of Rhode Island, Department of Mechanical, Industrial and Systems Engineering, Kingston, RI 02881, USA

[4]University of Virginia, Department of Materials Science and Engineering, Charlottesville, VA 22904, USA

[5]University of Virginia, Department of Physics, Charlottesville, VA 22904, USA

Supporting Information

ALD/MLD cycles:

ALD/MLD cycle sequences for our samples are in **Table S1**, they follow the formula $[(DEZ\text{-}H_2O)_{m+q} + (DEZ\text{-}HQ)]_n + (DEZ\text{-}H_2O)_{p.}$ with m,n,q and p being the cycle numbers. For superlattices n is always 0 because the distance between barrier layers stays constant, for example GM5(1)+50 200 nm: This is written as $[(DEZ\text{-}H_2O)_{75+50i} + (DEZ\text{-}HQ)]_5 + (DEZ\text{-}H_2O)_{325}$ with $i\epsilon(0,1,\ldots,4)$ in Table S1. This means that first 75(=m) + 50 (=q)*0 (i=0) cycles DEZ-H_2O are deposited, followed by a single DEZ-HQ cycle, this is repeated 5 (=n) times with *i* growing by one each cycle ($i\epsilon(0,1,\ldots,4)$). So after the first "round" there are 75 +50(=q)*1(i=1) = 125 DEZ-H_2O cycles before a benzene layer is introduced by one DEZ-HQ cycle again, this way the spacing is gradually increasing between the benzene layers before the last benzene layer is capped with 325 (=p) cycles of DEZ-H_2O.

The sandwich samples and the double benzene barrier do not fit into the $[(DEZ\text{-}H_2O)_{m+q} + (DEZ\text{-}HQ)]_n + (DEZ\text{-}H_2O)_p$ scheme and instead they have their cycle sequence explicitly written out.

E.g. SW SL5(1) 200 nm has the recipe 300 x (DEZ+H_2O) -> 5 x [100 x (DEZ+H_2O) + 1 x (DEZ +HQ)] -> 400 x (DEZ +H_2O). This indicates that first 300 cycles with diethylzinc and water were deposited (300 x (DEZ+H_2O)), followed by a superlattice sequence starting with 100 cycles DEZ and water and 1 cycle with diethylzinc and hydroquinone, which was repeated 5 times (5 x [100 x (DEZ+H_2O) + 1 x (DEZ +HQ)]) and finally 400 cycles of DEZ and water were deposited (400 x (DEZ +H_2O))

The table contains only samples that were made during this study and doesn't include samples from previously published articles.

Table S1: *The cycle sequences used to grow the newly reported samples.*

Sample name	m	n	p	q	Total cycles	Film thickness [nm]	Avg. ZnO layer thickness [nm]	Avg. GPC [Å]**
SL2(1) 50	110	2	110	0	332	45	14.7	1.35
SL3(1) 50	83	3	83	0	335	47	11.7	1.40
SL5(1) 50	55	5	55	0	335	49	7.8	1.46
SL5(1)b 100	95	5	95	0	575	90	15	1,57
SL12(1) 100	51	12	51	0	675	98	7.2	1.45
SL4(1) 100	132	4	132	0	664	97	19.1	1.46
SL3(1) 100	165	3	165	0	663	94	23.2	1.42
SL10(1) 100	59	10	59	0	659	94	8.2	1.43
SL8(1) 100	73	8	73	0	665	96	10.3	1.44
SL5(1) 200	195	5	195	0	1175	195	32	1.66
SL10(1) 200	110	10	110	0	1220	196	17	1.61
SL12(1) 200	102	12	102	0	1338	196	14.7	1.46
SL18(1) 200	70	18	70	0	1348	204	10.4	1.51
SL24(1) 200	50	24	50	0	1274	186	7.1	1.46
GM5(1)+50 200	75	5	325	50*i* with $i \in (0,1,\ldots,4)$	1205	205	34	1.7
GM10(1) +18 200	21	10	201	18*i* with $i \in (0,1,\ldots,9)$	1231	203	18	1.6
GM10(1) M±30 200	180	10	180	-30i with $i \in (0,1,\ldots,4,5,4,\ldots,1)$	1240	202	18	1.6

SW SL5(1) 200	300 x (DEZ+H_2O) -> 5 x [100 x (DEZ+H_2O) + 1 x (DEZ +HQ)] -> 400 x (DEZ +H2O)	1205	201	34	1.7
SW SL12(1) 200	335 x (DEZ+H_2O) -> 12 x [51 x (DEZ+H_2O) + 1 x (DEZ +HQ)] -> 385 x (DEZ +H_2O)	1344	190	15	1.4
Doublet 10(1) 200	5 x [170*(DEZ + H_2O) + 1 x (DEZ+H_2O) + 45*(DEZ+H_2O)+1 x (DEZ + HQ)]+ 170 + (DEZ +H_2O)	1250	210	19	1.7

Estimating the phonon mean free path in ZnO thin films:

The thermal conductivity due to phonons can be expressed in first approximation from kinetic theory as $\kappa_{Phon} = \frac{1}{3} C_V v l_{mfp}$. C_V being the heat capacity, v the average phonon velocity (approx. speed of sound) and l_{mfp} the mean free path[1] (page 122). We approximate $\kappa = \kappa_{Phon}$ in ZnO and with values for κ_{Phon} = 50 W m^{-1} K^{-1}, this value is estimated on the basis of Alvarez-Quintana et al.[2] who report 43 W m^{-1} K^{-1} for a 40 nm thick film and 56 W m^{-1} K^{-1} for a 180 nm thick film at 300K, the latter value is obtained by using the program plotreader[3] on their figure 4. The values of C_V = 2900 kj/m^3K and v are taken from Wu et al.[4]. For v we use 3700 m s^{-1} this has a great uncertainty as the speed of sound varies greatly depending on the crystal orientation it can be between 2760 - 6090 m/s, however choosing a value at the lower end of this spectrum seems wise considering we don't have a single crystal. We get

$$l_{mfp} = \frac{3\,\kappa_{Phon}}{C_v \times v} \approx \frac{3 \times 50\ J\,s^{-1}m^{-1}K^{-1}}{2900000\ J\,m^{-3}K^{-1} \times 3700\ m\,s^{-1}} \approx 14\ nm$$

This is a very simple calculation, that tends to underestimate the l_{mfp}, especially by approximating the phonon velocity v to the speed of sound. However it can be expected that the correct l_{mfp} is within an order of magnitude of the value estimated here.[5–7]

Thermal conductivity values of all reported samples in the ZnO/benzene system

In this study SL48(1) 100 and SL96(1) 100 were not used because those samples are amorphous (the spacing between the ZnO blocks is too small) and GM12(1) Fib 100 was also excluded because the ALD ZnO cycle sequence follows the Fibonacci sequence and the first few barrier layers are seperated by 1,1,2,3,5.. ALD cycles which is not enough to treat them seperately (as already discussed in [8] where this sample was first reported). We still list them in the table for the sake of completeness as there no other table to list the complete set.

SL5(1) 100 is an outlier (see multivariate analysis in the main text) and was not included in Figure 3 in the main text. We believe that SL5(b) 100 is the more representative sample of the two.

Table S2: *All reported thermal conductivity values of ZnO/benzene samples.*

Name	**Thickness (nm)**	**κ (W/mK)**	**Error**	**Source**
SL 6(1) 100	Ca. 100	7.2	n.a.	Tynell et al.[9]
SL 12(1) 100	Ca. 100	4.2	n.a.	Tynell et al.[9]
SL 6(1)b 100	91.1	6.9	1.4	Giri et al.[10]
SL 12(1)b 100	93.3	4.2	0.5	Giri et al.[10]
SL 24(1) 100	97.2	2.3	0.2	Giri et al.[10]
SL 48(1) 100*	93.8	0.8	0.15	Giri et al.[10]
SL 96(1) 100*	82.7	0.4	0.06	Giri et al.[10]
SL 12(3) 100	97	2.4	n.a.	Giri et al.[10]
SL 12(5) 100	97	1.6	n.a.	Giri et al.[10]
SL 12(7) 100	97	1.2	n.a.	Giri et al.[10]
SL 5(1) 100**	105	11.8	1.8	Krahl et al.[8]
SL 12(1)c 100	95	3.9	0.4	Krahl et al.[8]
GM 5(1) -20 100	115	9.3	0.9	Krahl et al.[8]
GM 5(1) +20 100	100	9.1	0.9	Krahl et al.[8]
GM 5(1) +20b 100	93	8.1	1.2	Krahl et al.[8]
GM 5(1) 20S 100	87	8.2	1.3	Krahl et al.[8]
GM 5(5) -20 100	125	4.1	0.3	Krahl et al.[8]
GM 12(1) +7 100	95	4.6	0.5	Krahl et al.[8]
GM 12(1) Fib 100*	95	7.9	1.1	Krahl et al.[8]
GM 12(1) M±8 100	92	3.2	0.3	Krahl et al.[8]
GM12(1) M±8 rev 100	92	3.3	0.3	Krahl et al.[8]
SW 1(12) 100	92	8.9	0.9	Krahl et al.[8]
Sl5(1)b 100	90	9.2	0.9	This publication
SL5(1) 200	195	10.0	1	This publication
SL10(1) 200	196	6.7	0.7	This publication
SW SL5(1) 200	201	9.5	1	This publication

GM5(1)+50 200	205	9.7	1	This publication
Doublet 10(1) 200	210	7.6	0.8	This publication
GM10(1) +18	203	7.3	0.7	This publication
GM 10(1) M±30 200	202	6.9	0.7	This publication
SL 12 (1)d 100	98	4.1	0.5	This publication
SL 12 (1) 200	196	6.7	0.8	This publication
SL 24 (1) 200	186	4.0	0.4	This publication
SW SL 12(1) 200	188	6.0	0.5	This publication
SL 18(1) 200	204	5.5	0.6	This publication
SL 10 (1) 100	94	4.4	0.6	This publication
SL 8(1) 100	96	5.6	0.8	This publication
SL 2(1) 50	45	8.9	5	This publication
SL 3(1) 50	47	6.9	3	This publication
SL 5 (1) 50	49	4.7	1	This publication
SL 4(1) 100	97	9.5	2	This publication
SL 3(1) 100	94	11.3	3	This publication

* Not used in this study, because amorphous (SL48(1) 100 and SL96(1) 100), or unclear layer separation (SL12(1) Fib 100).

** SL5(1) 100 is used in the Simca analysis but not in Figure 3, SL5(1)b 100 is considered the more representative sample.

An excel sheet with all variables used for the multivariate analysis can be obtained from the authors upon request.

Time domain thermoreflectance: modulation frequency and sensitivity

The measurement length scale of the TDTR technique is defined by the thermal penetration depth (TPD). Traditionally, thermal penetration depth is defined by the following equation:

$$\text{TPD} = \sqrt{\frac{k}{\pi C f}} \qquad \text{(Eq. S1)}$$

Here, *k, C* and *f* are thermal conductivity, volumetric heat capacity, and modulation frequency of the pump beam during TDTR measurements, respectively. However, thermal penetration depth calculated using this equation does not take into account the effects of the metal film transducer, the resulting thermal boundary conductance, the pump and probe spot size, and any finite thicknesses of films in multi-layer material systems. A more accurate representation of the thermal penetration depth can be obtained by solving the cylindrical heat diffusion equation, details of which were provided by Braun and Hopkins.[11] Though Eq. S1 does not provide an accurate value of the thermal penetration depth for the multilayered material systems, it qualitatively shows how TPD changes with modulation frequency. As the thickness of the films measured in this study range from ca. 50 to 200 nm, a high modulation frequency is desired during TDTR measurements. When the modulation frequency is high, the TPD is low. As a result, the sensitivity to the thin film thermal conductivity is higher compared to the substrate thermal conductivity. On the other hand, when the modulation frequency is low, the TPD is high and sensitivity to the substrate thermal conductivity is higher. This is shown by the sensitivity analysis of SL 12(1) 100 nm corresponding to 8.8 and 1 MHz in **Figure S2**. As shown in **Figure S2**, at 8.8 MHz, sensitivity to the thin film thermal conductivity is much larger than the substrate. Thus, using 8.8 MHz during TDTR measurements of the thin films, the influence and corresponding uncertainty propagation from the substrate thermal conductivity is minimized relative to that of lower modulation frequencies. Furthermore, in our current experimental setup, 8.8 MHz provides the best signal to noise ratio. That is why higher modulation frequencies (> 8.8 MHz) were avoided during the TDTR measurements.

In **Figure S3**, the thermal penetration depths for SL 12(1) 100 nm corresponding to 8.8 and 1 MHz have been provided. These thermal penetration depths have been calculated according to the definition provided by Braun and Hopkins.[11] As shown in **Figure S3** (a) and (b), the thermal penetration depths for 8.8 and 1 MHz are 180 and 800 nm, respectively. This further shows that at 8.8 MHz, we are most sensitive to the film thermal conductivity. However, with 1.1 MHz, as TDTR would probe more than 600 nm of the sapphire substrate, TDTR measurements at this frequency would be most sensitive to the substrate thermal conductivity.

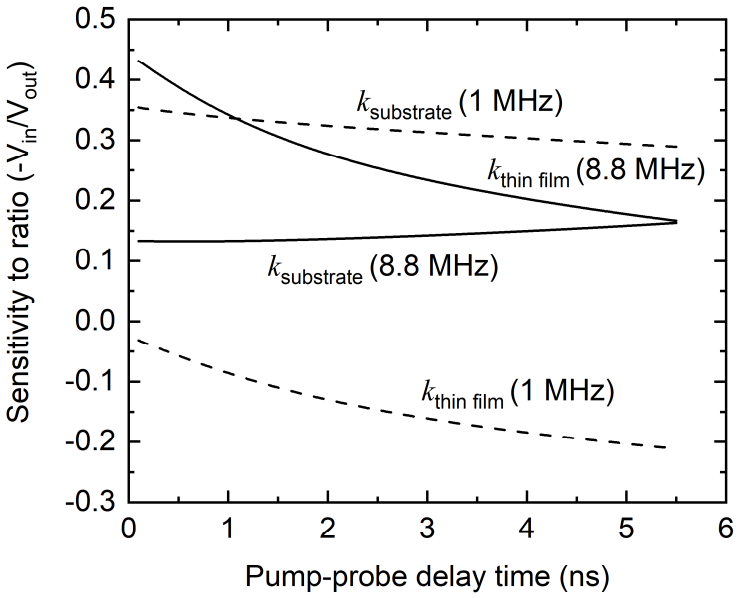

Figure S2: *Sensitivity of TDTR measurements to the substrate and thin film thermal conductivity of SL12(1) 100 for modulation frequencies of 8.8 and 1 MHz.*

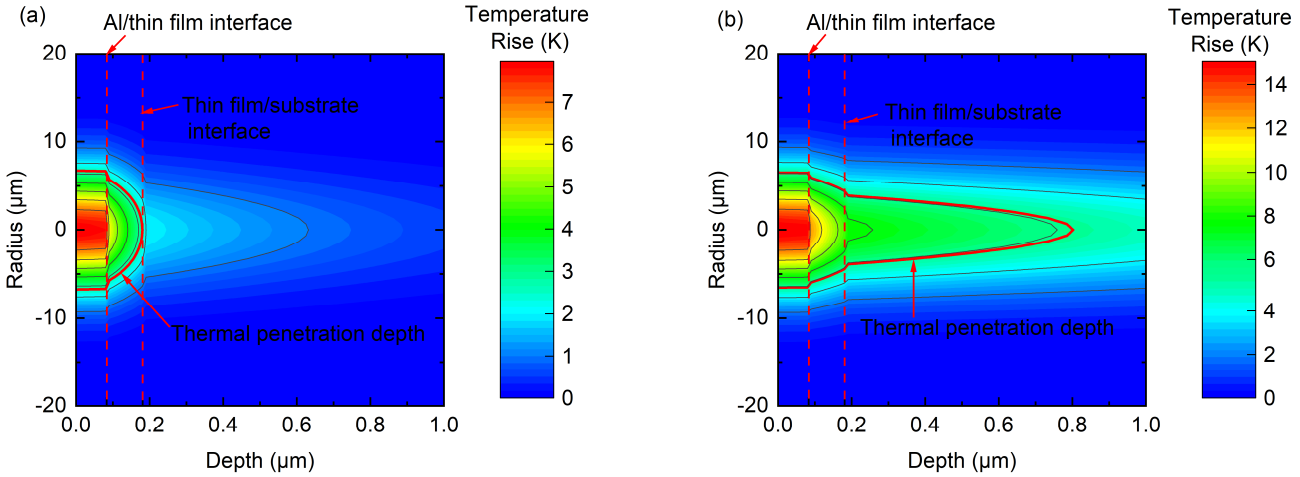

Figure S1*: Thermal penetration depth for SL12(1) 100 corresponding to (a) 8.8 MHz and (b) 1MHz modulation frequency. The temperature rise corresponds to a pump power of 30 mW.*

The sensitivity analysis of TDTR measurements for SL 12(1) 100 nm is shown in **Figure S4**. TDTR measurements are most sensitive to the transducer thickness and the thicknesses of the thin films. In this study, the thickness of the transducer and thin films were determined by picosecond acoustics and X-ray reflectivity, respectively. The uncertainty associated with the transducer and thin film thicknesses were ca. 3 and 5 nm, respectively. Due to the high modulation frequency (8.8 MHz) used during the TDTR measurements, sensitivity to the substrate thermal conductivity is minimal. TDTR measurements are almost insensitive to the

Al transducer thermal conductivity and Al/thin film thermal boundary conductance ($h_{Al/thin\ film}$). This means we have a high sensitivity towards the actual sample.

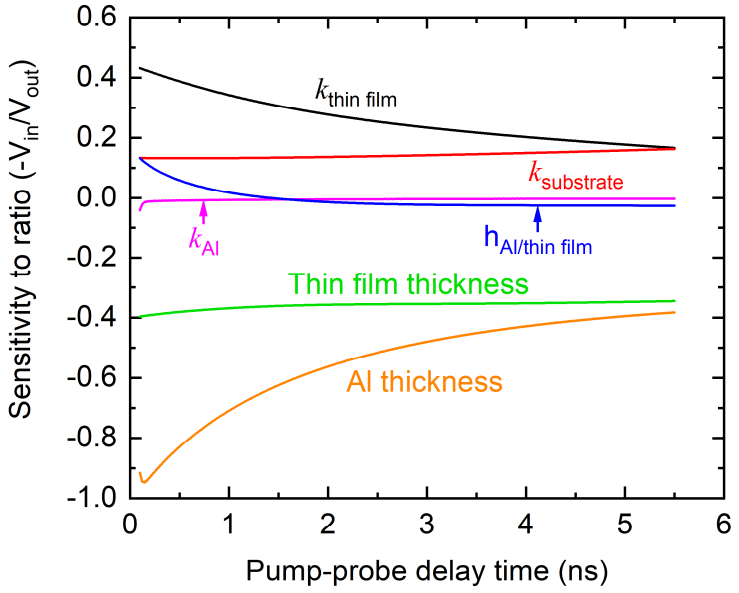

Figure S3: *Sensitivity to different parameters during TDTR measurement of SL12(1) 100.*

Supporting Information - References

(1) Kittel, C. *Introduction to Solid State Physics*, 8th Edition.; John Wiley & Sons, Inc.: New York, 2005.

(2) Alvarez-Quintana, J.; Martínez, E.; Pérez-Tijerina, E.; Pérez-García, S. A.; Rodríguez-Viejo, J. Temperature Dependent Thermal Conductivity of Polycrystalline ZnO Films. *J. Appl. Phys.* 2010, *107*, 063713. https://doi.org/10.1063/1.3330755.

(3) Bruggeman, J. *PlotReader*. version 1.55.0.0. https://jornbr.home.xs4all.nl/plotreader/. 2010

(4) Wu, X.; Lee, J.; Varshney, V.; Wohlwend, J. L.; Roy, A. K.; Luo, T. Thermal Conductivity of Wurtzite Zinc-Oxide from First-Principles Lattice Dynamics – a Comparative Study with Gallium Nitride. *Sci. Rep.* 2016, *6*, 22504.

(5) Regner, K. T.; Sellan, D. P.; Su, Z.; Amon, C. H.; McGaughey, A. J. H.; Malen, J. A. Broadband Phonon Mean Free Path Contributions to Thermal Conductivity Measured Using Frequency Domain Thermoreflectance. *Nat. Commun.* 2013, *4*, 1640. https://doi.org/10.1038/ncomms2630.

(6) Henry, A. S.; Chen, G. Spectral Phonon Transport Properties of Silicon Based on Molecular Dynamics Simulations and Lattice Dynamics. *J. Comp. Theor. Nanosci.* 2008, *5*, 141–152. https://doi.org/10.1166/jctn.2008.2454.

(7) Ju, Y. S.; Goodson, K. E. Phonon Scattering in Silicon Films with Thickness of Order 100 Nm. *Appl. Phys. Lett.* 1999, *74*, 3005–3007. https://doi.org/10.1063/1.123994.

(8) Krahl, F.; Giri, A.; Tomko, J. A.; Tynell, T.; Hopkins, P. E.; Karppinen, M. Thermal Conductivity Reduction at Inorganic–Organic Interfaces: From Regular Superlattices to Irregular Gradient Layer Sequences. *Adv. Mater. Interfaces* 2018, *5*, 1701692. https://doi.org/10.1002/admi.201701692.

(9) Tynell, T.; Giri, A.; Gaskins, J.; Hopkins, P. E.; Mele, P.; Miyazaki, K.; Karppinen, M. Efficiently Suppressed Thermal Conductivity in ZnO Thin Films via Periodic Introduction of Organic Layers. *J. Mater. Chem. A* 2014, *2*, 12150–12152. https://doi.org/10.1039/C4TA02381A.
(10) Giri, A.; Niemelä, J.-P.; Tynell, T.; Gaskins, J. T.; Donovan, B. F.; Karppinen, M.; Hopkins, P. E. Heat-Transport Mechanisms in Molecular Building Blocks of Inorganic/Organic Hybrid Superlattices. *Phys. Rev. B* 2016, *93*, 115310. https://doi.org/10.1103/PhysRevB.93.115310.
(11) Braun, J. L.; Hopkins, P. E. Upper Limit to the Thermal Penetration Depth during Modulated Heating of Multilayer Thin Films with Pulsed and Continuous Wave Lasers: A Numerical Study. *J. Appl. Phys.* 2017, *121*, 175107. https://doi.org/10.1063/1.4982915.